Biophysical Journal, Volume *121*

Supplemental information

The structural basis of BCR-ABL recruitment of GRB2 in chronic myelogenous leukemia

Yonglan Liu, Hyunbum Jang, Mingzhen Zhang, Chung-Jung Tsai, Ryan Maloney, and Ruth Nussinov

The structural basis of BCR-ABL recruitment of GRB2 in chronic myelogenous leukemia

Yonglan Liu[a], Hyunbum Jang[b], Mingzhen Zhang[b], Chung-Jung Tsai[b], Ryan Maloney[a] and Ruth Nussinov[b,c,*]

[a]Computational Structural Biology Section, Cancer Innovation Laboratory, National Cancer Institute, Frederick, MD 21702, U.S.A.

[b]Computational Structural Biology Section, Cancer Innovation Laboratory, Frederick National Laboratory for Cancer Research, Frederick, MD 21702, U.S.A.

[c]Department of Human Molecular Genetics and Biochemistry, Sackler School of Medicine, Tel Aviv University, Tel Aviv 69978, Israel

Author for correspondence:

Tel: 301-846-5579

E-mail: NussinoR@mail.nih.gov

The authors declare no potential conflicts of interest.

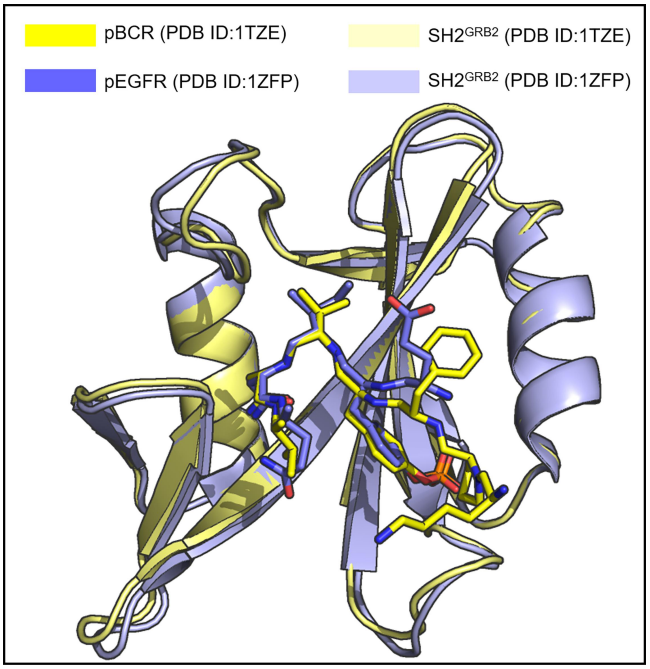

Figure S1. Superimposition of the conformations from the two different crystal structures of $SH2^{GRB2}$ in complex with pBCR ($_{174}$KPFpYVNV$_{180}$) (PDB ID: 1TZE) and pEGFR ($_{1067}$EpYINQ$_{1071}$) (PDB ID: 1ZFP) peptides. $SH2^{GRB2}$ shown as cartoon is colored light yellow and light blue in complex with pBCR and pEGFR, respectively. Both pBCR and pEGFR peptides shown as sticks are colored yellow and blue, respectively.

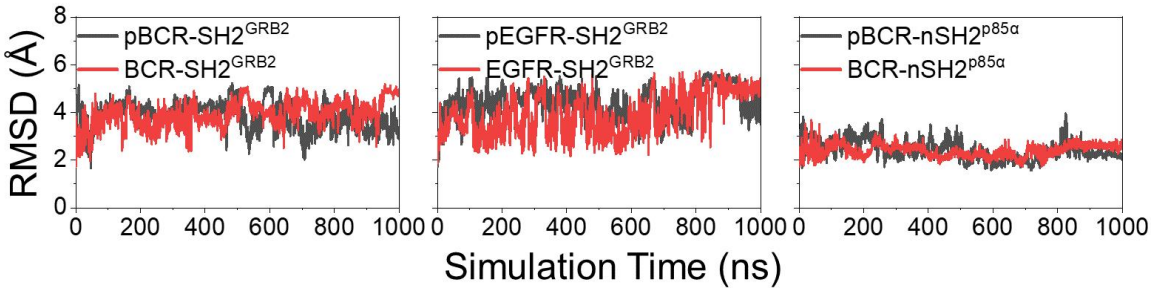

Figure S2. Time evolution of root-mean-square deviations (RMSDs) for pBCR–$SH2^{GRB2}$ and BCR–$SH2^{GRB2}$, pEGFR–$SH2^{GRB2}$ and EGFR–$SH2^{GRB2}$, and pBCR–$nSH2^{p85\alpha}$ and BCR–$nSH2^{p85\alpha}$.

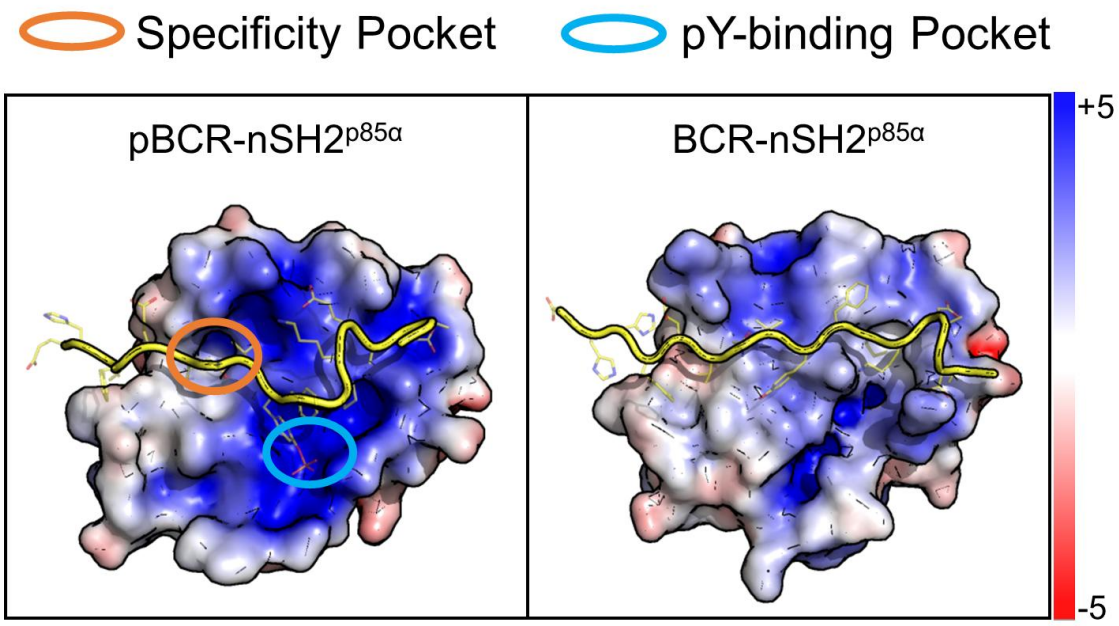

Figure S3. Binding modes of pBCR–nSH2$^{p85\alpha}$ and BCR–nSH2$^{p85\alpha}$ systems. nSH2$^{p85\alpha}$ shown as electrostatic surface is colored based on the charge properties (red, negative charge; blue, positive charge), characterizing the electrostatic surfaces of nSH2$^{p85\alpha}$. The peptides shown as tubes are colored yellow. The cartoon structures of protein represent the averaged structures over the last half of the simulations. The representative structures account for 63.6% and 60.8 % of the ensemble structures over the last half of the trajectories for pBCR–nSH2$^{p85\alpha}$ and BCR–nSH2$^{p85\alpha}$, respectively.

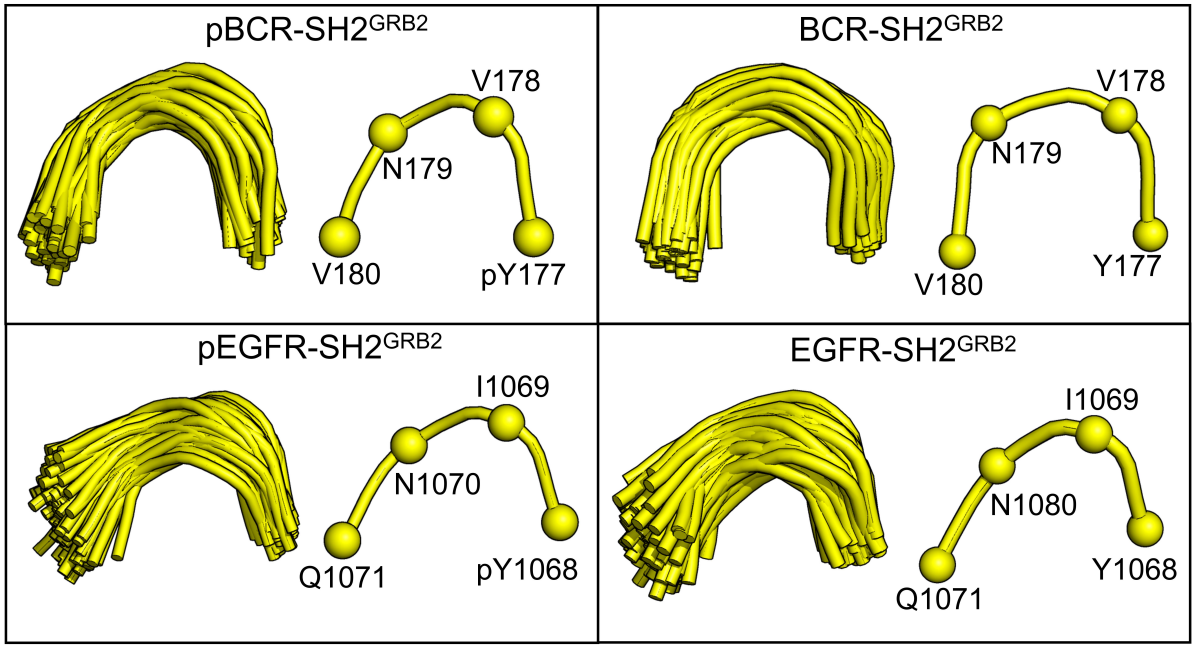

Figure S4. Structural alignment (left) of the type I β-turn region (residues from the pY position to the +3 position C-terminal to pY) and the representative conformation of type I β-turn (right) for each peptide in the bound state for the pBCR-SH2^{GRB2}, BCR-SH2^{GRB2}, pEGFR-SH2^{GRB2}, and EGFR-SH2^{GRB2} systems. In the cartoons, the peptides are shown as tubes. In the representative conformations, spheres denote the Cα atoms of β-turn residues. These residues are marked on each peptide. Superimpositions of the aligned structures were obtained from the last half of the simulations.

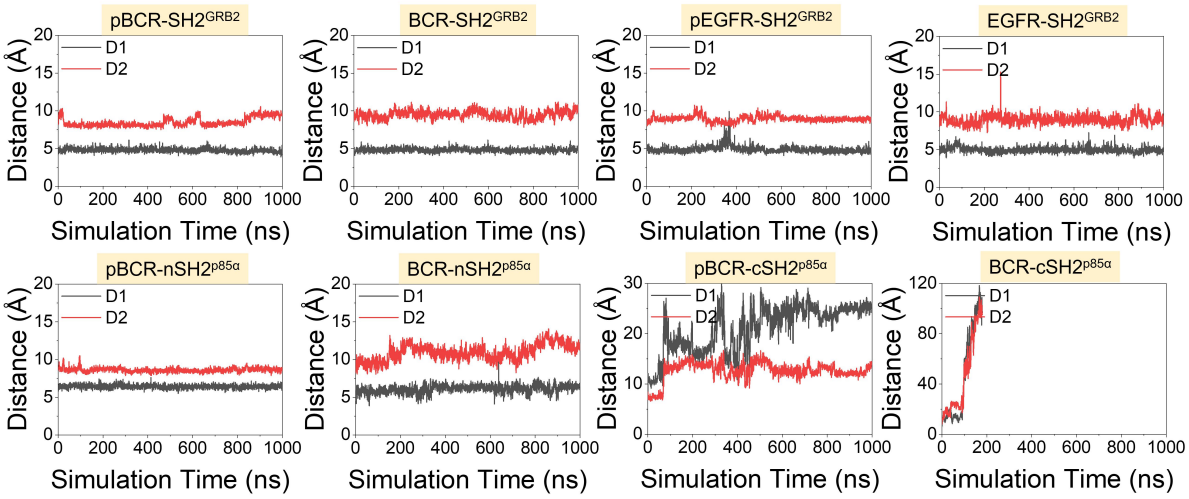

Figure S5. Time evolution of D1 and D2 for pBCR–SH2^{GRB2} and BCR–SH2^{GRB2}, pEGFR–SH2^{GRB2} and EGFR–SH2^{GRB2}, and pBCR–nSH2$^{p85\alpha}$ and BCR–nSH2$^{p85\alpha}$, and pBCR–cSH2$^{p85\alpha}$ and BCR–cSH2$^{p85\alpha}$. D1 is the distance between the Cα atom of N179 in pBCR/BCR, or N1070 in pEGFR/EGFR, and the center of mass of the Cα atoms of the residues (F108, K109, L120, and W121 in SH2^{GRB2}; I381, F392, Y416, and N417 in nSH2$^{p85\alpha}$; and C670, F681, H706, and L710 in cSH2$^{p85\alpha}$) forming the specificity pocket of the SH2 domains. D2 is the distance between the Cα atom of pY177 in pBCR, Y177 in BCR, pY1068 in pEGFR, or Y1068 in EGFR, and the Cα atoms of the residues (R67, R86, S88, S90, S96, H107, and K109 in SH2^{GRB2}; R340, R358, S361, T362, K382, and L380 in nSH2$^{p85\alpha}$; and R631, R639, H669, and V671 in cSH2$^{p85\alpha}$) forming the pY-binding pocket of the SH2 domains.

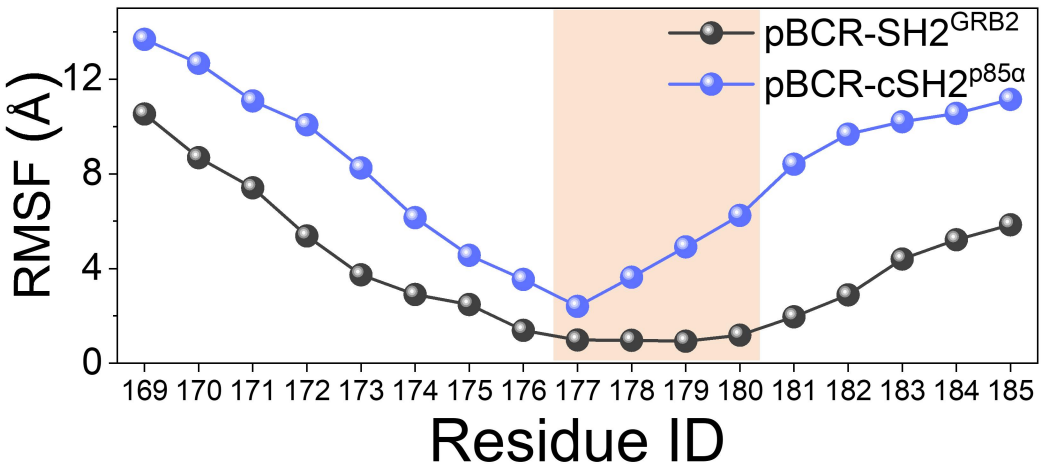

Figure S6. Root-mean-square fluctuations (RMSFs) of pBCR in the pBCR-SH2^{GRB2} and pBCR-cSH2$^{p85\alpha}$ systems. RMSFs are calculated for the last half of the simulations.

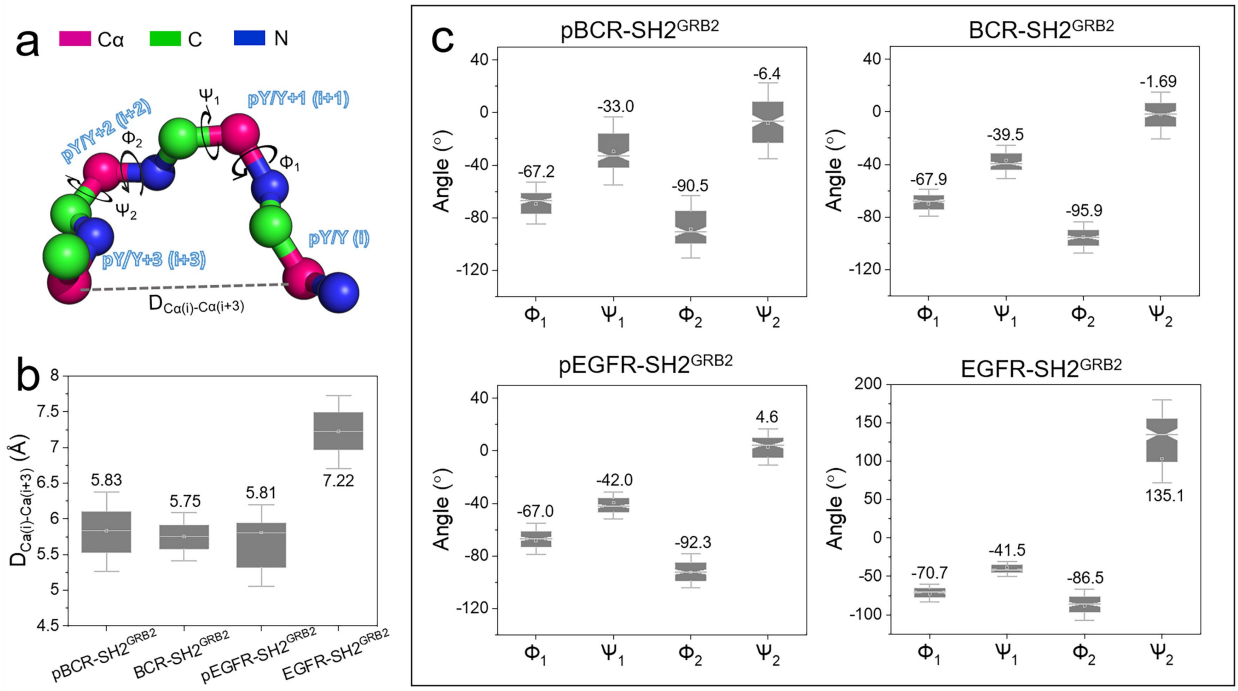

Figure S7. Characterization of type I β-turn conformation of pY/Y-peptides in complex with $SH2^{GRB2}$. (a) Definition of $D_{Cα(i)-Cα(i+3)}$ and the torsion angles of ϕ_1, ψ_1, ϕ_2, and ψ_2. (b) $D_{Cα(i)-Cα(i+3)}$ and (c) ϕ_1, ψ_1, ϕ_2, and ψ_2 of the peptides in pBCR–$SH2^{GRB2}$, BCR–$SH2^{GRB2}$, pEGFR–$SH2^{GRB2}$, and EGFR–$SH2^{GRB2}$.

a

Affinity order	0	1	2	3
1	pY	V	N	I
2	pY	E	N	V
3	pY	V	N	V
4	pY	K	N	I
5	pY	V	N	Q
6	pY	Q	N	L
6	pY	I	N	A
8	pY	K	N	L
8	pY	M	N	M
10	pY	I	N	Q

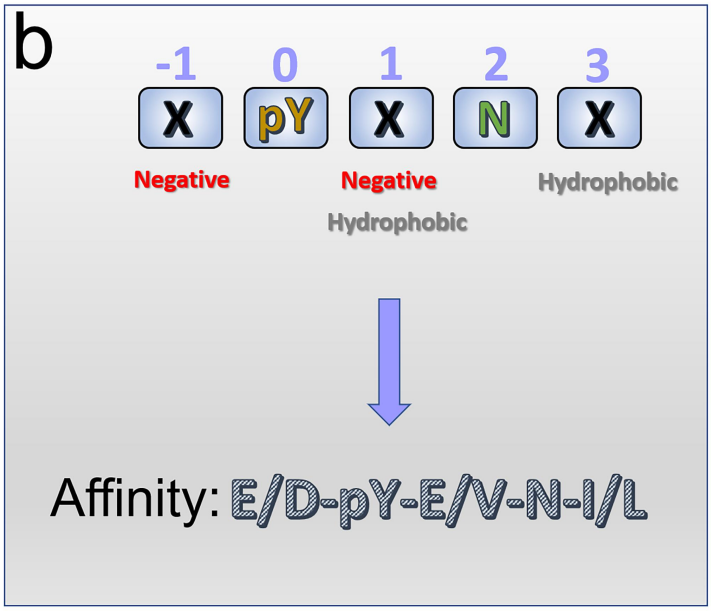

Figure S8. (a) $SH2^{GRB2}$-binding motifs collected from literatures. The motifs are sorted in the decreasing order of binding affinity to $SH2^{GRB2}$. (b) Putative five-residue motifs for the binding of $SH2^{GRB2}$ with the optimal binding affinity.

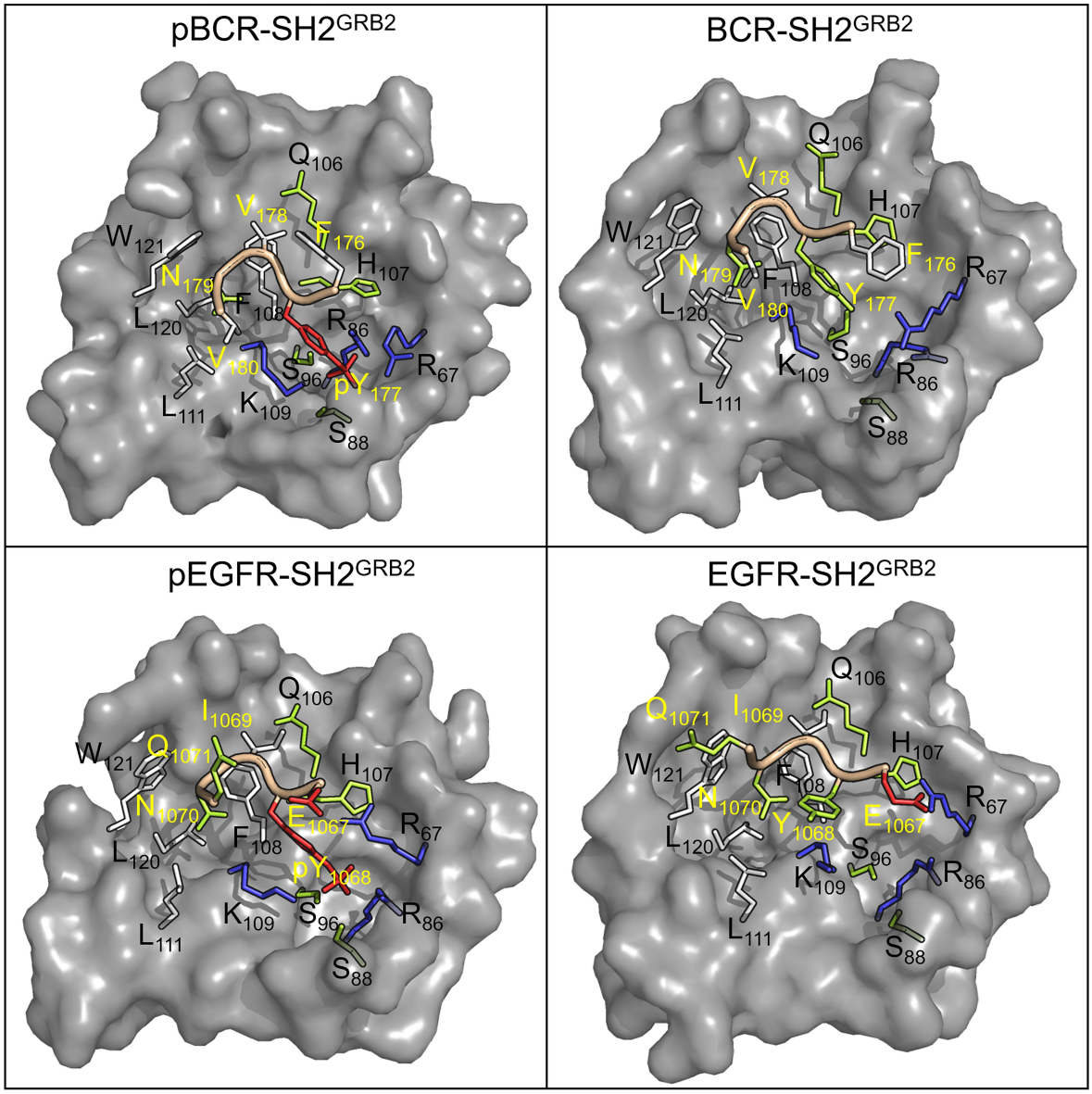

Figure S9. Interaction interfaces of pBCR–SH2^{GRB2}, BCR–SH2^{GRB2}, pEGFR–SH2^{GRB2}, and EGFR–SH2^{GRB2} systems. Interfacial residues are shown as sticks. Hydrophobic, hydrophilic, positively charged, and negatively charged residues are colored white, green, blue, and red, respectively. The yellow and black labels denote the peptide and SH2^{GRB2} residues, respectively.

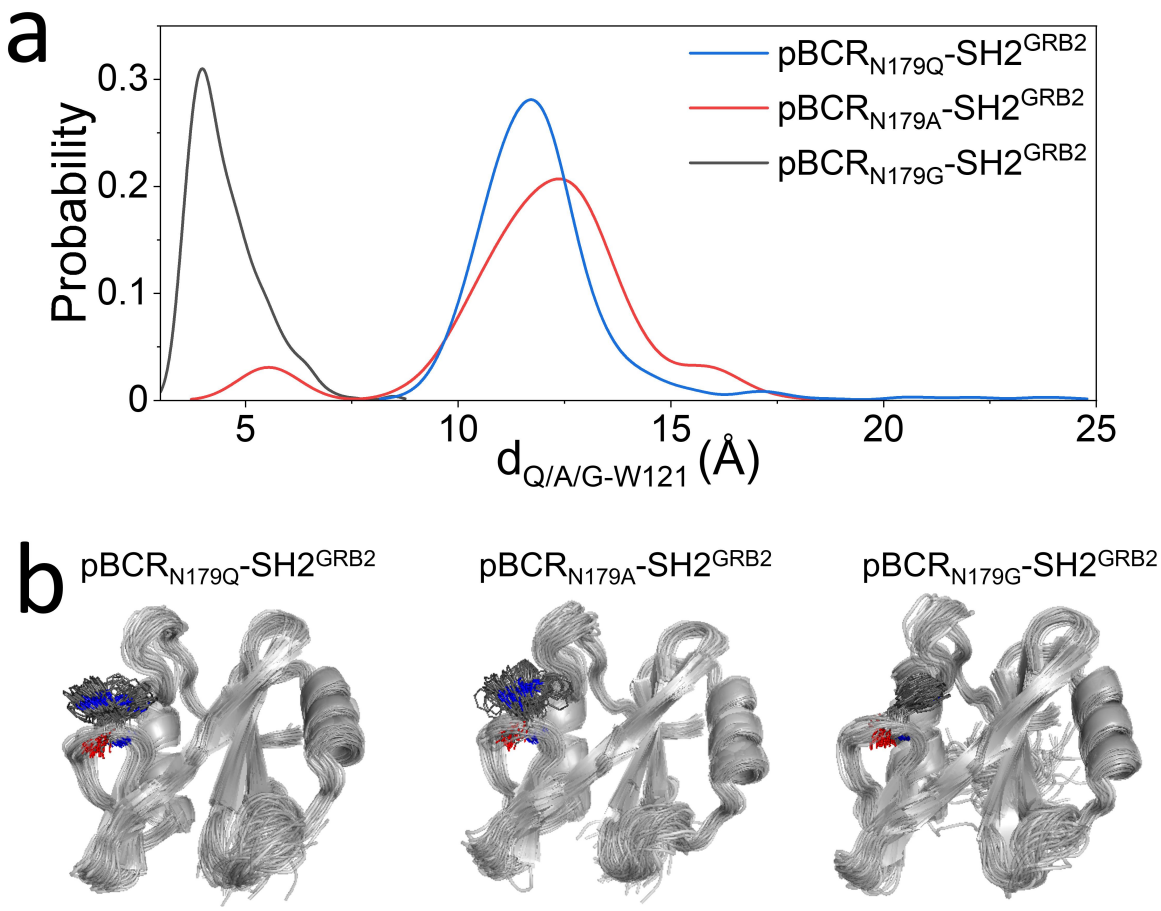

Figure S10. (a) Probability distribution functions of the distance between W121 in $SH2^{GRB2}$ and Q179/A179/G179 in $pBCR_{N179Q}$/$pBCR_{N179A}$/$pBCR_{N179G}$, $d_{Q/A/G-W121}$, and (b) superimposed snapshots representing the dynamic behaviors of W121 sidechain for $pBCR_{N179Q}$–$SH2^{GRB2}$, $pBCR_{N179A}$–$SH2^{GRB2}$, and $pBCR_{N179G}$–$SH2^{GRB2}$.

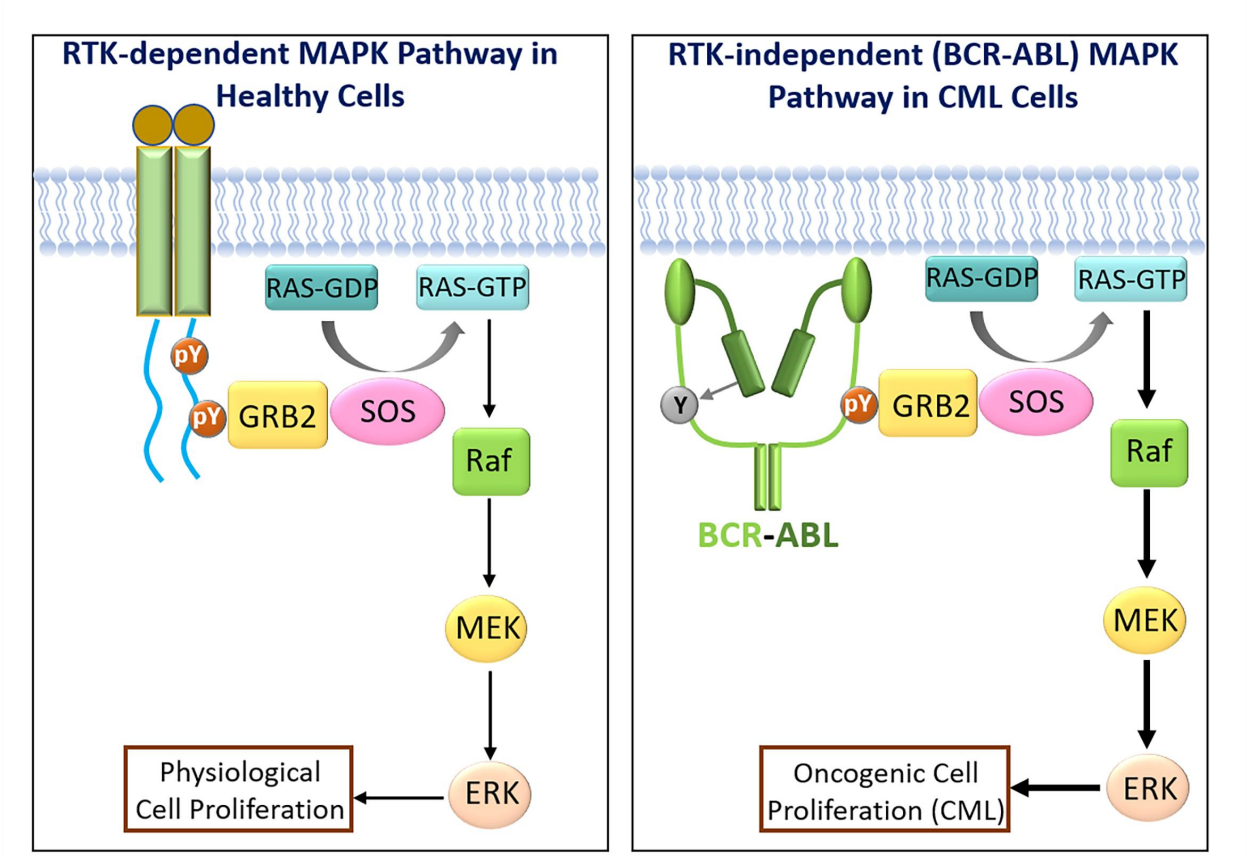

Figure S11. Schematic illustration of RTK-dependent in healthy cells and BCR-ABL-dependent Ras/MAPK signaling pathways in CML cells.

Table S1. Intermolecular pair residues with contact probability >=60% for pY/Y–SH2^{GRB2} systems.

pBCR-SH2^{GRB2}	BCR-SH2^{GRB2}	pEGFR-SH2^{GRB2}	EGFR-SH2^{GRB2}
F176-H107	F176-R67	E1067-R67	E1067-H107
pY177-R67	F176-H107	E1067-H107	Y1068-S96
pY177-R86	Y177-S96	pY1068-R67	Y1068-H107
pY177-S88	Y177-H107	pY1068-R86	Y1068-F108
pY177-S96	Y177-F108	pY1068-S88	Y1068-K109
pY177-H107	Y177-K109	pY1068-S96	I1069-Q106
pY177-F108	V178-Q106	pY1068-H107	I1069-H107
pY177-K109	V178-H107	pY1068-F108	I1069-F108
V178-Q106	V178-F108	pY1068-K109	I1069-W121
V178-H107	V178-W121	I1069-Q106	I1069-S141
V178-F108	V178-S141	I1069-H107	N1070-F108
N179-F108	N179-F108	I1069-F108	N1070-K109
N179-K109	N179-K109	I1069-W121	N1070-L111
N179-L111	N179-L111	N1070-F108	N1070-L120
N179-L120	N179-L120	N1070-K109	N1070-W121
N179-W121	N179-W121	N1070-L111	
V180-K109	V180-K109	N1070-L120	
V180-L111	V180-L111	N1070-W121	
F182-W121	E185-R67		
E185-R142			

Table S2. pY-peptides of different proteins with affinity to the $SH2^{GRB2}$ domain.

Protein Name	pTyr Peptide Sequence	Reference
BCR	$_{174}$KPFpYVNV$_{180}$	(1)
EGFR	$_{1067}$EpYINQ$_{1071}$	(2)
β-PDGFR	$_{701}$LQHHSDKRRPPSAELpYSNALPVG$_{723}$	(3)
DF3	$_{1243}$pYTNP$_{1246}$	(4)
SIT	$_{90}$pYGNL$_{93}$	(5)
SIT	$_{188}$pYANS$_{191}$	(5)
IRS-1	$_{891}$SPGEpYVNIEFGS$_{902}$	(6)
SHC	$_{314}$DPSpYVNVNQNL$_{324}$	(6)
SHC	$_{236}$DHQpYYND$_{242}$	(7)
SHP2	$_{542}$pYTNI$_{545}$	(8)
SHP2	$_{584}$pYENV$_{587}$	(9)
FAK	$_{924}$VpYENV$_{928}$	(10)
c-MET	$_{1356}$pYVNV$_{1359}$	(11)
c-Kit/SCFR	$_{694}$QEDHAEAALpYKNLLHSKESS$_{713}$	(12)
c-Kit/SCFR	$_{928}$ISESTNHIpYSNLANCSPNR$_{946}$	(12)
CD28	$_{188}$HSDpYMNMTPR$_{197}$	(13,14)
AICD	$_{679}$QNGpYENPTY$_{687}$	(15)
Modified AICD	$_{679}$QNGpYVNPTY$_{687}$	(15)
LAT	$_{108}$ASpYENE$_{113}$	(16)
LAT	$_{125}$DDpYHNP$_{130}$	(16)
LAT	$_{169}$DDpYVNV$_{174}$	(16)

LAT	$_{189}$REpYVNV$_{194}$	(16)
LAT	$_{224}$PDpYENL$_{229}$	(16)
PLD2	$_{168}$NpYLNR$_{172}$	(17)
PLD2	$_{178}$FpYRNY$_{182}$	(17)
HER2/Neu	$_{1138}$EpYVNQ$_{1142}$	(18)

Table S3. Intermolecular pair residues with interaction energies <-20 kcal/mol for pY/Y-peptide–SH2^{GRB2} systems.

pBCR–SH2^{GRB2}	Energy (kcal/mol)	BCR–SH2^{GRB2}	Energy (kcal/mol)	pEGFR–SH2^{GRB2}	Energy (kcal/mol)	EGFR–SH2^{GRB2}	Energy (kcal/mol)
pY177-R67	-138.35±3.85	E185-R67	-63.64±20.64	pY1068-R67	-128.26±4.64	E1067-R67	-40.59±4.90
pY177-R86	-127.18±2.66	E185-R86	-29.01±7.12	pY1068-R86	-95.83±5.23		
pY177-K109	-144.68±5.61	E185-K109	-59.05±17.37	pY1068-K109	-154.9±8.45		
pY177-S88	-27.29±3.31			pY1068-S88	-29.73±2.33		
pY177-S90	-26.11±2.58			E1067-R67	-49.14±3.48		
pY177-S96	-28.51±2.79						
E185-R142	-78.82±15.89						

Table S4. Hydrogen bonds between residues in $SH2^{GRB2}$ domain and residues in pBCR, BCR, pEGFR, and EGFR.

System	Donor	Acceptor	Occupancy (%)
pBCR–$SH2^{GRB2}$	$R67^{GRB2}$-S	$pY177^{pBCR}$-S	100.00
	$R86^{GRB2}$-S	$pY177^{pBCR}$-S	100.00
	$S88^{GRB2}$-S	$pY177^{pBCR}$-S	69.36
	$S90^{GRB2}$-S	$pY177^{pBCR}$-S	54.80
	$S96^{GRB2}$-S	$pY177^{pBCR}$-S	99.04
	$K109^{GRB2}$-S	$pY177^{pBCR}$-S	90.56
	$V178^{pBCR}$-B	$H107^{GRB2}$-B	92.56
	$K109^{GRB2}$-B	$N179^{pBCR}$-S	95.60
	$N179^{pBCR}$-S	$K109^{GRB2}$-B	97.60
	$N179^{pBCR}$-S	$L120^{GRB2}$-B	86.08
BCR–$SH2^{GRB2}$	$V178^{BCR}$-B	$H107^{GRB2}$-B	91.60
	$N179^{BCR}$-S	$K109^{GRB2}$-B	97.12
	$K109^{GRB2}$-B	$N179^{BCR}$-S	94.40
	$N179^{BCR}$-S	$L120^{GRB2}$-B	86.40
	$R67^{GRB2}$-S	$E185^{BCR}$-S	59.36
pEGFR–$SH2^{GRB2}$	$R67^{GRB2}$-S	$pY1068^{pEGFR}$-S	98.40
	$R86^{GRB2}$-S	$pY1068^{pEGFR}$-S	85.04
	$S88^{GRB2}$-S	$pY1068^{pEGFR}$-S	93.52
	$S96^{GRB2}$-S	$pY1068^{pEGFR}$-S	82.40
	$K109^{GRB2}$-S	$pY1068^{pEGFR}$-S	98.64

	I1069^{pEGFR}-B	H107^{GRB2}-B	87.44
	N1070^{pEGFR}-S	K109^{GRB2}-B	97.44
	K109^{GRB2}-B	N1070^{pEGFR}-S	97.44
	N1070^{pEGFR}-S	L120^{GRB2}-B	85.76
EGFR–SH2^{GRB2}	I1069^{EGFR}-B	H107^{GRB2}-B	86.64
	K109^{GRB2}-B	N1070^{EGFR}-S	94.56
	N1070^{EGFR}-S	K109^{GRB2}-B	89.28
	N1070^{EGFR}-S	L120^{GRB2}-B	76.24

Hydrogen bonds listed in the table have the occupancy > 50% during last 500-ns simulations. S and B indicate sidechain and backbone of residues.

References

1. Rahuel, J., B. Gay, D. Erdmann, A. Strauss, C. Garcia-Echeverria, P. Furet, G. Caravatti, H. Fretz, J. Schoepfer, and M. G. Grutter. 1996. Structural basis for specificity of Grb2-SH2 revealed by a novel ligand binding mode. *Nat Struct Biol*. 3(7):586-589.
2. Rahuel, J., C. Garcia-Echeverria, P. Furet, A. Strauss, G. Caravatti, H. Fretz, J. Schoepfer, and B. Gay. 1998. Structural basis for the high affinity of amino-aromatic SH2 phosphopeptide ligands. *J Mol Biol*. 279(4):1013-1022.
3. Arvidsson, A. K., E. Rupp, E. Nanberg, J. Downward, L. Ronnstrand, S. Wennstrom, J. Schlessinger, C. H. Heldin, and L. Claessonwelsh. 1994. Tyr-716 in the Platelet-Derived Growth-Factor Beta-Receptor Kinase Insert Is Involved in Grb2 Binding and Ras Activation. *Molecular and Cellular Biology*. 14(10):6715-6726.
4. Pandey, P., S. Kharbanda, and D. Kufe. 1995. Association of the DF3/MUC1 breast cancer antigen with Grb2 and the Sos/Ras exchange protein. *Cancer Res*. 55(18):4000-4003.
5. Pfrepper, K. I., A. Marie-Cardine, L. Simeoni, Y. Kuramitsu, A. Leo, J. Spicka, I. Hilgert, J. Scherer, and B. Schraven. 2001. Structural and functional dissection of the cytoplasmic domain of the transmembrane adaptor protein SIT (SHP2-interacting transmembrane adaptor protein). *Eur J Immunol*. 31(6):1825-1836.
6. Skolnik, E. Y., C. H. Lee, A. Batzer, L. M. Vicentini, M. Zhou, R. Daly, M. J. Myers, Jr., J. M. Backer, A. Ullrich, M. F. White, and et al. 1993. The SH2/SH3 domain-containing protein GRB2 interacts with tyrosine-phosphorylated IRS1 and Shc: implications for insulin control of ras signalling. *EMBO J*. 12(5):1929-1936.
7. Harmer, S. L., and A. L. DeFranco. 1997. Shc contains two Grb2 binding sites needed for efficient formation of complexes with SOS in B lymphocytes. *Mol Cell Biol*. 17(7):4087-4095.
8. Bennett, A. M., T. L. Tang, S. Sugimoto, C. T. Walsh, and B. G. Neel. 1994. Protein-tyrosine-phosphatase SHPTP2 couples platelet-derived growth factor receptor beta to Ras. *Proc Natl Acad Sci U S A*. 91(15):7335-7339.
9. Vogel, W., and A. Ullrich. 1996. Multiple in vivo phosphorylated tyrosine phosphatase SHP-2 engages binding to Grb2 via tyrosine 584. *Cell Growth Differ*. 7(12):1589-1597.
10. Schlaepfer, D. D., S. K. Hanks, T. Hunter, and P. van der Geer. 1994. Integrin-mediated signal transduction linked to Ras pathway by GRB2 binding to focal adhesion kinase. *Nature*. 372(6508):786-791.
11. Schiering, N., E. Casale, P. Caccia, P. Giordano, and C. Battistini. 2000. Dimer formation through domain swapping in the crystal structure of the Grb2-SH2-Ac-pYVNV complex. *Biochemistry*. 39(44):13376-13382.
12. Thömmes, K., J. Lennartsson, M. CARLBERG, and L. Rönnstrand. 1999. Identification of Tyr-703 and Tyr-936 as the primary association sites for Grb2 and Grb7 in the c-Kit/stem cell factor receptor. *Biochemical Journal*. 341(1):211-216.
13. Higo, K., T. Ikura, M. Oda, H. Morii, J. Takahashi, R. Abe, and N. Ito. 2013. High resolution crystal structure of the Grb2 SH2 domain with a phosphopeptide derived from CD28. *PLoS One*. 8(9):e74482.
14. Schneider, H., Y. C. Cai, K. V. Prasad, S. E. Shoelson, and C. E. Rudd. 1995. T cell antigen CD28 binds to the GRB-2/SOS complex, regulators of p21ras. *Eur J Immunol*. 25(4):1044-1050.
15. Das, S., M. Raychaudhuri, U. Sen, and D. Mukhopadhyay. 2011. Functional Implications of the Conformational Switch in AICD Peptide upon Binding to Grb2-SH2 Domain. *Journal of Molecular Biology*. 414(2):217-230.

16. Cho, S., C. A. Velikovsky, C. P. Swaminathan, J. C. Houtman, L. E. Samelson, and R. A. Mariuzza. 2004. Structural basis for differential recognition of tyrosine-phosphorylated sites in the linker for activation of T cells (LAT) by the adaptor Gads. *EMBO J*. 23(7):1441-1451.
17. Di Fulvio, M., N. Lehman, X. Lin, I. Lopez, and J. Gomez-Cambronero. 2006. The elucidation of novel SH2 binding sites on PLD2. *Oncogene*. 25(21):3032-3040.
18. Dankort, D., N. Jeyabalan, N. Jones, D. J. Dumont, and W. J. Muller. 2001. Multiple ErbB-2/Neu phosphorylation sites mediate transformation through distinct effector proteins. *Journal of Biological Chemistry*. 276(42):38921-38928.